Variable Temperature Study of the Cross-Relaxation Dynamics in the Hyperpolarized Xenon-Induced Enhancement of Surface Nuclei

Luis J. Smith, Jay Smith, Ernesto MacNamara, Kevin Knagge, and Daniel Raftery*

H. C. Brown Laboratory, Department of Chemistry, Purdue University, West Lafayette, Indiana 47907-1393

Received: September 13, 2000; In Final Form: December 15, 2000

The cross-relaxation rate constants for a three spin system involving hyperpolarized ^{129}Xe, ^{13}C, and ^{1}H nuclei have been determined over a wide temperature range (136−216 K) through observation of the polarization enhancements from spin polarization induced nuclear Overhauser effect (SPINOE) experiments. A model system of methoxy groups adsorbed on high surface area silica was studied. A maximum polarization enhancement of 3.4 was observed for the methoxy carbon. Xenon−carbon and xenon−proton cross-relaxation were found to be dependent on both the xenon coverage and xenon diffusion across the silica surface. The temperature dependence of the cross-relaxation rate constants was effectively fit using a hopping model. Possible improvements for the SPINOE experiment are suggested including alternative substrates which would retard xenon diffusion across the surface and improve xenon−carbon cross-relaxation leading to significantly larger SPINOE enhancements.

Introduction

Solid-state nuclear magnetic resonance (SSNMR) has long been recognized as a powerful method for the study of materials. The inherent elemental selectivity of the technique allows for structural and kinetic investigations of a wide range of chemical systems. However SSNMR is a notoriously insensitive technique due to the low Boltzmann factor at room temperature and the broad lines typically observed. To compensate for the low sensitivity, large amounts of sample are used in order to maximize the available signal. The sensitivity problem is even more pronounced for surface studies, as the signal arising from the small number of spins on the surface of a material represents a small fraction of the observed signal emanating primarily from the bulk. Nevertheless, SSNMR can provide valuable surface information on such high surface area samples as catalysts and porous materials.[1−12] It is therefore of broad interest to pursue methods to enhance the surface signal. One of the most promising methods is the use of optical pumping, pioneered by Happer and co-workers,[13] for the hyper-polarization of noble gases. Optical pumping of ^{129}Xe and ^{3}He creates spin polarizations that are 4 to 5 orders of magnitude higher than thermal polarization.[14−16] The large gain in polarization and thus signal intensity has created opportunities in a range of fields including medical imaging, physics, and materials science.[17−27] To combine the enhanced signals of the hyperpolarized noble gases with the elemental selectivity of NMR, efforts have been made to transfer the high noble gas polarization to other nuclei. Among the developed methods utilizing hyperpolarized ^{129}Xe are high-field Hartmann−Hahn cross polarization,[28,29] low-field thermal mixing,[30,31] and the spin polarization induced nuclear Overhauser effect (SPINOE).[32] Of these three methods, SPINOE yields enhancements that are the simplest to achieve experimentally, and has been used extensively to date.[33−42]

SPINOE occurs because the large spin polarization of the xenon drives an incoherent polarization transfer to a target nucleus via cross-relaxation in the laboratory frame. As the polarization of the xenon is created by optical pumping, no pulses are required to create the initial state to drive the transfer. Only a pulse to observe the enhancement of the heteronuclear magnetization is necessary, thus simplifying the technique. In addition, magic-angle spinning (MAS) can be applied easily to further improve the spectral resolution.[34,36] To achieve sizable enhancements of surface nuclei, the method requires that significant amounts of hyperpolarized xenon reside on the surface. As a result, low temperatures are required to ensure a large enhancement, which does result in some experimental difficulties. While low temperatures are known to be necessary, the complete temperature dependence of the various cross-relaxation pathways is not well-known. An understanding of the temperature dependence of the relaxation pathways involved in SPINOE should clarify the limitations and the potential of SPINOE as a signal enhancement technique.

To study the dynamics of the spin polarization transfer, a model system has been created utilizing methanol chemisorbed, i.e., methoxy groups, on high surface area silica. In an earlier paper,[41] we conducted a study involving this sample at a single low temperature (147 K). In that study we determined the rate constants for the relaxation pathways and observed that the combination of SPINOE and NOE resulted in enhancements superior to cross polarization, particularly for deuterated samples where the signal enhancement was 25 times larger than the room-temperature ^{13}C spectrum. In the present paper, the relevant cross- and auto-relaxation rate parameters have been determined for the SPINOE enhancement of the methoxy carbon over a larger temperature range from 136 to 216 K. Through the determination of the temperature dependence of the relevant relaxation parameters, we have clarified the role of the various parameters that are involved in the SPINOE enhancement, which will aid in maximizing the utility of the SPINOE method for surface signal enhancement.

Theory

The interaction of xenon with the surface methoxy groups results in an interaction involving three different nuclei, (xenon,

* Corresponding author. Fax: +1-765-494-0239. E-mail: raftery@purdue.edu.

10.1021/jp0032309 CCC: $20.00
Published on Web 01/30/2001

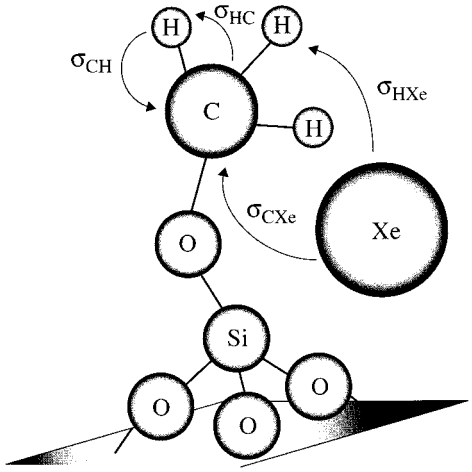

Figure 1. Schematic drawing showing the cross-relaxation pathways (σ) among surface ^{1}H, ^{13}C, and ^{129}Xe nuclei for a methoxylated silica surface.

carbon, and protons) as shown in Figure 1. The xenon atoms adsorbed on the surface contact the protons and carbon atoms through dipolar coupling. The protons and carbon atoms interact as well via dipolar coupling. The time-dependent nature of the couplings, which is the result of the hopping of the xenon atom across the surface and the rotation of the methyl and methoxy groups, allows for cross-relaxation between the atoms. Time-dependent dipolar interactions are necessary for the nuclear Overhauser effect (and SPINOE) to occur. The observed enhancements result from the relative magnitude of the cross-relaxation rates, σ, and the auto-relaxation rates, ρ. Three experiments that measure the time-dependent nature of the NOE enhancements determine the various rates for the diverse relaxation pathways denoted in Figure 1. Only three cross-relaxation rates need be determined to fully characterize the spin polarization transfer dynamics: σ_{HXe}, cross-relaxation between xenon atoms and protons; σ_{CXe}, cross-relaxation between xenon and carbon atoms; and σ_{CH}, cross-relaxation between protons and carbon atoms.[41,43] The polarization transfer that results from the various cross-relaxation and auto-relaxation rates are described by the Solomon equations, here modified to account for the continuous flow of xenon across the surface:

$$\frac{d\eta_C}{dt} = -\rho_C\cdot\eta_C - \sigma'_{CH}\cdot\eta_H - \sigma'_{CXe}\cdot\eta_{Xe}$$

$$\frac{d\eta_H}{dt} = -\rho_H\cdot\eta_H - \sigma'_{HC}\cdot\eta_C - \sigma'_{HXe}\cdot\eta_{Xe} \qquad (1)$$

$$\frac{d\eta_{Xe}}{dt} = -\rho^{eff}_{Xe}\cdot\eta_{Xe} + \rho^{OP}_{Xe}\cdot\eta^{OP}_{Xe} - \sigma'_{XeC}\cdot\eta_C - \sigma'_{XeH}\cdot\eta_H$$

$\eta_I(t)$ is the time-dependent polarization enhancement of the I magnetization defined as

$$\eta_I = \frac{(I(t) - I_0)}{I_0} \qquad (2)$$

where I_0 is the Boltzmann equilibrium polarization at the given temperature and $I(t)$ is the observed signal. σ' is defined as

$$\sigma'_{IS} = \frac{\gamma_S}{\gamma_I}\cdot\frac{S\cdot(S+1)}{I\cdot(I+1)}\cdot\sigma_{IS} \qquad (3)$$

and is used to make the theoretical description of the polarization enhancement less cumbersome. The σ' term is simply a scaling of the cross-relaxation rate based on the gyromagnetic ratios and the nuclear spin of the coupled nuclei, I and S. We note that we are not at this point relating σ_{IS} and σ_{SI} (see below). The ρ_C and ρ_H terms are the auto-relaxation rate constants for the ^{13}C and ^{1}H nuclei. For the time-dependent xenon polarization enhancement, two auto-relaxation terms are used to account for continuous flow. The auto-relaxation rate constant of the xenon, ρ^{eff}_{Xe}, describes the combination of the polarization loss due to relaxation of adsorbed xenon at the surface as well as loss of xenon as it flows out of the rotor. The additional rate, ρ^{OP}_{Xe}, describes the growth of polarization due to the flow of hyperpolarized xenon into the rotor.

Under the conditions of continuous flow of hyperpolarized xenon, the spin polarization on the surface reaches a steady-state condition. The surface xenon polarization, η^{SS}_{Xe}, can be defined for the steady state by rearranging the third differential equation in eq 1:

$$\eta^{SS}_{Xe} = \frac{-\sigma'_{XeC}\cdot\eta_C - \sigma'_{XeH}\cdot\eta_H + \rho^{OP}_{Xe}\cdot\eta^{OP}_{Xe}}{\rho^{eff}_{Xe}} \qquad (4)$$

The rate constants for cross-relaxation between ^{129}Xe atoms and the ^{1}H and ^{13}C atoms are very small and are dwarfed by the rate at which xenon flows into the rotor, ρ^{OP}_{Xe}. A flow of thermally polarized or hyperpolarized xenon will result in the product $\rho^{OP}_{Xe}\cdot\eta^{OP}_{Xe}$ dominating the numerator. The differences in the magnitude of the terms allows the surface xenon polarization enhancement to be approximated by

$$\eta^{SS}_{Xe} \approx \frac{\rho^{OP}_{Xe}\cdot\eta^{OP}_{Xe}}{\rho^{eff}_{Xe}} \qquad (5)$$

The replacement of the xenon polarization by a constant term, η^{SS}_{Xe}, reduces the number of Solomon equations to two, thus simplifying the problem considerably. In addition, continuous flow of xenon removes the dependence of the Solomon equations on xenon auto-relaxation which is now accounted for in the xenon steady-state surface polarization enhancement.

Three transient NOE experiments were performed. To determine the cross-relaxation rate constant between carbon and protons, a transient NOE experiment is performed under thermally polarized xenon flow. The interaction of the carbon nuclei with the adsorbed xenon can act as an additional relaxation mechanism. It is important to conduct the experiment under continuous xenon flow in order to ensure that the measured auto-relaxation rate constant for the carbon nuclei is consistent with the later experiments conducted with a continuous flow of hyperpolarized xenon. The pulse sequence is shown in Figure 2a. With the cross-relaxation rate constant σ'_{CXe} having a much smaller value than σ'_{CH} (see below), the effect of the low xenon polarization can be neglected in the Solomon equation for η_C. The equation to describe Experiment I becomes:

$$\frac{d\eta_C}{dt} = -\rho_C\cdot\eta_C + \sigma'_{CH} \qquad (6)$$

The solution using the initial condition created by the pulse train, $\eta_C(0) = -1$, results in

$$\eta_C(\tau) = -\left(\frac{\sigma'_{CH}}{\rho_C} + 1\right)\cdot e^{-\rho_C\cdot\tau} + \frac{\sigma'_{CH}}{\rho_C} \qquad (7a)$$

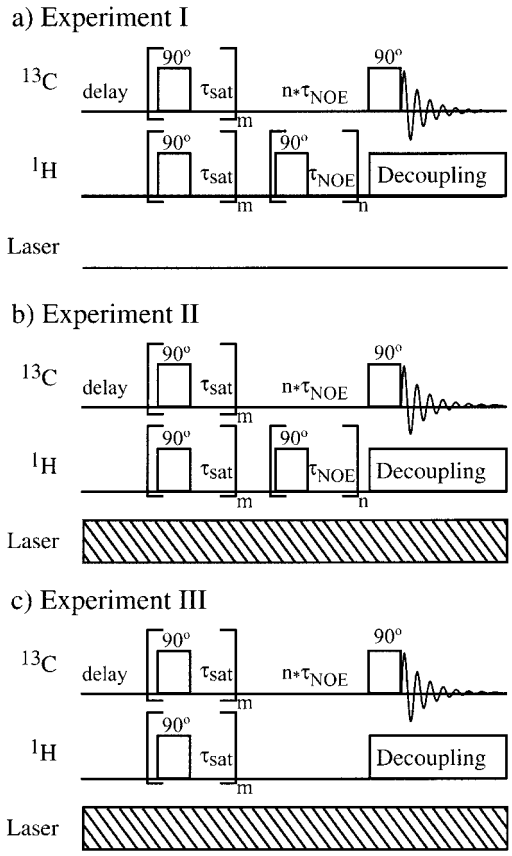

Figure 2. The NOE pulse sequences used in the variable temperature study for Experiments I (a), II (b), and III (c). For all experiments: $\tau_{sat} = 10$ ms, $\tau_{NOE} = 10$ ms, $m = 100$, and n was varied from 10 to 3000.

or

$$\eta_C(\tau) = \left(-\frac{\gamma_H}{\gamma_C}\cdot\frac{\sigma_{CH}}{\rho_C} - 1\right)\cdot e^{-\rho_C\cdot\tau} + \frac{\gamma_H}{\gamma_C}\cdot\frac{\sigma_{CH}}{\rho_C} \qquad (7b)$$

with $S = I = {}^1/_2$, and a steady-state polarization enhancement of

$$\eta_C(\infty) = \frac{\gamma_H}{\gamma_C}\cdot\frac{\sigma_{CH}}{\rho_C} \qquad (8)$$

Extraction of the xenon−carbon cross-relaxation rate constant can be easily achieved through a modification of Experiment I. In the second experiment, the laser is turned on, and the gas flow over the modified silica surface consists of hyperpolarized xenon. The pulse sequence is shown in Figure 2b. Since the xenon nuclei are now hyperpolarized, the contribution from cross-relaxation involving xenon cannot be neglected. Using the xenon steady-state surface polarization enhancement approximation, the Solomon equations for Experiment II can be written as:

$$\frac{d\eta_C}{dt} = -\rho_C\cdot\eta_C + \sigma'_{CH} - \sigma'_{CXe}\cdot\eta_{Xe}^{SS} \qquad (9)$$

The solution to this differential equation, using the initial condition $\eta_C(0) = -1$, is

$$\eta_C(\tau) = \left(\frac{\sigma'_{CXe}\cdot\eta_{Xe}^{SS} - \sigma'_{CH}}{\rho_C} - 1\right)\cdot e^{-\rho_C\cdot\tau} - \frac{\sigma'_{CXe}\cdot\eta_{Xe}^{SS} + \sigma'_{CH}}{\rho_C} \qquad (10a)$$

or

$$\eta_C(\tau) = \left(\frac{\gamma_{Xe}}{\gamma_C}\cdot\frac{\sigma_{CXe}\cdot\eta_{Xe}^{SS}}{\rho_C} - \frac{\gamma_H}{\gamma_C}\cdot\frac{\sigma_{CH}}{\rho_C} - 1\right)\cdot e^{-\rho_C\cdot\tau} - \frac{\gamma_{Xe}}{\gamma_C}\cdot\frac{\sigma_{CXe}\cdot\eta_{Xe}^{SS}}{\rho_C} + \frac{\gamma_H}{\gamma_C}\cdot\frac{\sigma_{CH}}{\rho_C} \qquad (10b)$$

with the steady-state polarization enhancement of the carbon described by

$$\eta_C(\infty) = -\frac{\gamma_{Xe}}{\gamma_C}\cdot\frac{\sigma_{CXe}\cdot\eta_{Xe}^{SS}}{\rho_C} + \frac{\gamma_H}{\gamma_C}\cdot\frac{\sigma_{CH}}{\rho_C} \qquad (11)$$

Equation 11 shows that the enhancement is the result of the sum of the carbon−proton NOE and the xenon−carbon SPINOE.

The last cross-relaxation rate constant of interest, σ_{HXe}, can be measured simply by eliminating the saturation pulse train applied to the protons during the time period τ. The pulse sequence for Experiment III is shown in Figure 2c. As in Experiment II, the sample is exposed to a continuous gas flow of hyperpolarized xenon. We use a steady-state approximation to describe the xenon spins to simplify the problem. The Solomon equations that describe Experiment III are

$$\frac{d\eta_C}{dt} = -\rho_C\cdot\eta_C - \sigma'_{CH}\cdot\eta_H - \sigma'_{CXe}\cdot\eta_{Xe}^{SS}$$

$$\frac{d\eta_H}{dt} = -\rho_H\cdot\eta_H - \sigma'_{HC}\cdot\eta_C - \sigma'_{HXe}\cdot\eta_{Xe}^{SS} \qquad (12)$$

yielding a set of two inhomogeneous differential equations. The solution to the homogeneous problem, when $\eta_{Xe}^{SS} = 0$, is well-known:[44]

$$\eta_C(\tau) = c_1\cdot e^{\lambda_1\cdot\tau} + c_2\cdot e^{\lambda_2\cdot\tau}$$

$$\eta_H(\tau) = c_1\cdot\left(\frac{\rho_C + \lambda_1}{-\sigma'_{CH}}\right)\cdot e^{\lambda_1\cdot\tau} + c_2\cdot\left(\frac{\rho_C + \lambda_2}{-\sigma'_{CH}}\right)\cdot e^{\lambda_2\cdot\tau} \qquad (13)$$

where λ_1 and λ_2 are defined accordingly:

$$\lambda_1 = \frac{-(\rho_C + \rho_H) - \sqrt{(\rho_C - \rho_H)^2 + 4\cdot\sigma'_{CH}\cdot\sigma'_{HC}}}{2}$$

$$\lambda_2 = \frac{-(\rho_C + \rho_H) + \sqrt{(\rho_C - \rho_H)^2 + 4\cdot\sigma'_{CH}\cdot\sigma'_{HC}}}{2} \qquad (14)$$

The carbon to proton cross-relaxation rate constant, σ'_{HC}, is determined according to ref 43. The methyl group protons are closest; the next-nearest methoxy or hydroxyl species are very distant (see below) and can be ignored and thus N_H/N_C is set equal to three. From the solution to the homogeneous problem, the solution to the inhomogeneous one is derived. Using the method of variation of parameters,[45] a general solution can be found. The solution to this new set of differential equations yields the general solution, which results from the addition of $a_1\cdot e^{\lambda_1\cdot\tau}$ and $a_2\cdot e^{\lambda_2\cdot\tau}$ to the solution of the homogeneous problem in which:

$$a_1 = \frac{-(\rho_C + \lambda_2)\cdot\sigma'_{CXe}\cdot\eta^{SS}_{Xe} - \sigma'_{CH}\cdot\sigma'_{HXe}\cdot\eta^{SS}_{Xe}}{\lambda_1\cdot(\lambda_1 - \lambda_2)}\cdot e^{-\lambda_1\cdot\tau}$$

$$a_2 = \frac{-(\rho_C + \lambda_1)\cdot\sigma'_{CXe}\cdot\eta^{SS}_{Xe} - \sigma'_{CH}\cdot\sigma'_{HXe}\cdot\eta^{SS}_{Xe}}{-\lambda_2\cdot(\lambda_1 - \lambda_2)}\cdot e^{-\lambda_2\cdot\tau} \quad (15)$$

Using the initial conditions of Experiment III, the time-dependent polarization enhancement of the carbon spins is

$$\eta_C(\tau) = \left(\frac{\rho_C + \lambda_2 + \sigma'_{CH}}{\lambda_1 - \lambda_2} + \eta_1\right)\cdot e^{\lambda_1\cdot\tau} + \left(\frac{-\rho_C - \lambda_1 - \sigma'_{CH}}{\lambda_1 - \lambda_2} + \eta_2\right)\cdot e^{\lambda_2\cdot\tau} - \eta_1 - \eta_2 \quad (16)$$

where

$$\eta_1 = \frac{(\rho_C + \lambda_2)\cdot\sigma'_{CXe}\cdot\eta^{SS}_{Xe} + \sigma'_{CH}\cdot\sigma'_{HXe}\cdot\eta^{SS}_{Xe}}{\lambda_1\cdot(\lambda_1 - \lambda_2)}$$

$$\eta_2 = \frac{-(\rho_C + \lambda_1)\cdot\sigma'_{CXe}\cdot\eta^{SS}_{Xe} - \sigma'_{CH}\cdot\sigma'_{HXe}\cdot\eta^{SS}_{Xe}}{\lambda_2\cdot(\lambda_1 - \lambda_2)} \quad (17)$$

The steady-state polarization enhancement of the carbon atoms is

$$\eta_C(\infty) = -\eta_1 - \eta_2 = -\frac{\rho_H\cdot\sigma'_{CXe}\cdot\eta^{SS}_{Xe}}{\rho_C\cdot\rho_H - \sigma'_{CH}\cdot\sigma'_{HC}} + \frac{\sigma'_{CH}\cdot\sigma'_{HXe}\cdot\eta^{SS}_{Xe}}{\rho_C\cdot\rho_H - \sigma'_{CH}\cdot\sigma'_{HC}} \quad (18a)$$

or

$$\eta_C(\infty) = -\left(\frac{\gamma_{Xe}}{\gamma_C}\cdot\frac{\rho_H\cdot\sigma_{CXe}\cdot\eta^{SS}_{Xe}}{(\rho_C\cdot\rho_H - \sigma_{CH}\cdot\sigma_{HC})}\right) + \left(\frac{\gamma_H}{\gamma_C}\cdot\frac{\gamma_{Xe}}{\gamma_H}\cdot\frac{\sigma_{CH}\cdot\sigma_{HXe}\cdot\eta^{SS}_{Xe}}{(\rho_C\cdot\rho_H - \sigma_{CH}\cdot\sigma_{HC})}\right) \quad (18b)$$

In the case where $\sigma_{CH} \ll \rho_C, \rho_H$, an approximation can be made for the steady-state polarization enhancement of the carbon. (This approximation was used in our previous work[41] and also set the relaxation rates λ_1 and λ_2 equal to $-\rho_C$ and $-\rho_H$, respectively.)

$$\eta_C(\infty) = -\frac{\gamma_{Xe}}{\gamma_C}\cdot\frac{\sigma_{CXe}\cdot\eta^{SS}_{Xe}}{\rho_C} + \frac{\gamma_{Xe}}{\gamma_C}\cdot\frac{\sigma_{CH}\cdot\sigma_{HXe}\cdot\eta^{SS}_{Xe}}{\rho_C\cdot\rho_H} \quad (19)$$

The resulting polarization equation shows that the enhancement of the carbon spins results from the sum of the xenon−carbon SPINOE and a combination of the proton−carbon NOE and the xenon−proton SPINOE. By comparing this result to the result of Experiment II (eq 11), one can see that the combination is a scaling of the proton−carbon NOE by the SPINOE between the protons and xenon. These two terms in eq 19 are always in competition due to the difference in sign which reduces the overall enhancement. Even if the signs of the gyromagnetic ratios of the three different nuclei involved are not the same, the two terms that make up the steady-state polarization remain opposite in sign.

Experimental Section

Hyperpolarized ^{129}Xe was produced using an optical pumping apparatus similar to the one designed by Driehuys[46] for the production of large quantities of polarized gas under continuous flow conditions. A schematic is shown in Figure 3. The pumping cell is situated on a laser table approximately 3 m from the high-field magnet. A magnetic field of approximately 20 G across the pumping cell is provided by a small set of Helmholtz coils. The light source is a 25 W fiber-optic coupled diode laser centered at 795 nm (OptoPower Corp., Tucson, AZ). The optical pumping gas mixture, consisting of 96% helium, 2% nitrogen, and 2% natural abundance xenon (26% ^{129}Xe) is introduced into the pumping cell at 6 atm. The cell is heated to 140 °C to vaporize sufficient quantities of rubidium to interact with the xenon. A monochromator and CCD camera located after the pumping cell allows for the monitoring of the rubidium adsorption line. A Teflon needle valve located after the pumping cell drops the pressure to 1 atm and provides flow control. The flow rate used in this study was approximately 100 mL/min. Glass tubing connects the pumping cell to the sample chamber in our modified commercial CP-MAS probe. We use a small glass injection tube to deliver the polarized gas mixture to the sample rotor based on methods developed by Hunger and Horvath.[47] As this tube, used to introduce the xenon to the sample, is in contact with the cold nitrogen gas exiting the probe, the xenon is quite cold when it reaches the sample region. All glass surfaces in contact with xenon were coated with SurfaSil (Pierce Chemicals) to minimize xenon polarization losses through wall-induced relaxation. A Kel-F holder situated on the top of the rotor housing supports the injection tube, which fits into the rotor through a small hole that was drilled into the rotor cap. The xenon gas-phase polarization[48] for the variable temperature study was 4.5% as measured by comparison to a thermally polarized xenon standard (see below).

All NMR experiments were performed on an extensively modified Chemagnetics spectrometer using a Tecmag Aries pulse programmer and data acquisition system. The spectrometer operated at ^{1}H, ^{13}C, and ^{129}Xe frequencies of 200.3, 50.44, and 55.47 MHz, respectively. A modified Varian 7 mm variable temperature CP-MAS probe was used. Variable temperature operation was performed using nitrogen as the bearing and drive gas with the bearing gas being pre-cooled using a liquid nitrogen bath. For all experiments, the sample was spun at 3 kHz. The thermocouple inside the CP-MAS probe was calibrated using $Pb(NO_3)_2$.[49] The error in the temperature measurements was estimated to be ±1 K.

Methoxylated silica samples were prepared from fumed silica, Cab-O-Sil (Grade M-5, Cabot Corporation), and carbon-13 labeled methanol (Cambridge Isotopes). The silica was dehydrated for 4 h at 140 °C under vacuum (10^{-4} Torr) and then exposed to 0.70 mmol of the methanol followed by heating at 400 °C for 3 h. The sample was then evacuated to 1×10^{-4} Torr to remove excess methanol. Subsequently, 25 mg of the sample was loaded into a NMR MAS rotor and spun. Between experiments, the sample was stored in normal room air.

Xenon adsorption isotherms were made using a standard vacuum manifold equipped with mechanical and diffusion pumps. The sample was under a vacuum of 10^{-5} Torr for ~10 h. Adsorption measurements were made using pressure values ranging from 10 Torr to 650 Torr. At each pressure point, the system was allowed to equilibrate for 3 to 4 min. Equilibration was considered to be achieved when the pressure variation was less than 0.2 Torr. Low-temperature baths consisting of organic solvent/liquid nitrogen mixtures were used to maintain temperature. Adsorption isotherms were collected at 167, 170, 184, 197, and 213 K.

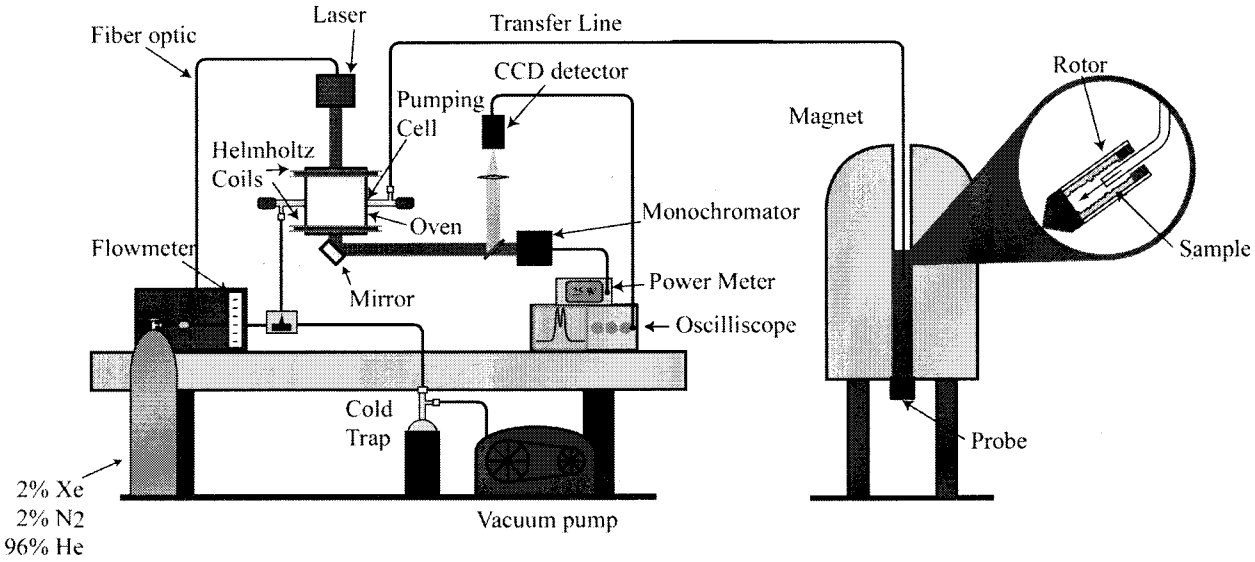

Figure 3. Schematic diagram of the experimental setup for the production and continuous delivery of hyperpolarized xenon gas to the MAS rotor.

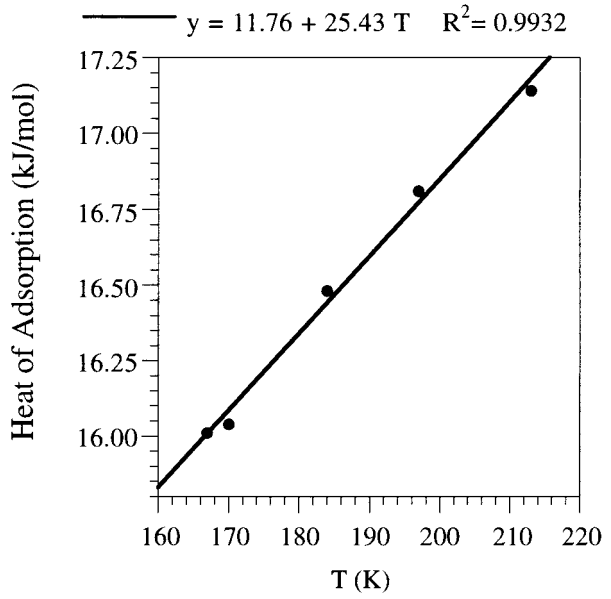

Figure 4. Variation with temperature in the heat of adsorption of xenon on methoxylated silica. The heats of adsorption were determined from BET isotherms (see text).

Results

Xenon coverage of the surface of the methoxylated silica was calculated from adsorption data using BET theory.[50] The heat of adsorption for xenon on the treated silica was determined from the BET isotherms and used to extrapolate the heats for the temperatures studied. As shown in Figure 4, a linear dependence on temperature was observed for the heats of adsorption. The calculated xenon coverage as a function of temperature is shown in Figure 5a. As expected, the coverage of the surface decreases dramatically with increasing temperature. Surface coverage under our experimental conditions of 15 Torr of xenon partial pressure varied from 73% of a monolayer at 136 K to 3% at 216 K.

Variable temperature ^{129}Xe MAS NMR spectra allowed the determination of the surface polarization. Two peaks are observed in the MAS spectra at all the temperatures studied: a gas-phase peak set at 0 ppm and an adsorbed peak whose chemical shift changes with temperature (from 102 ppm at 216 K to 155 ppm at 136 K). With increasing coverage and

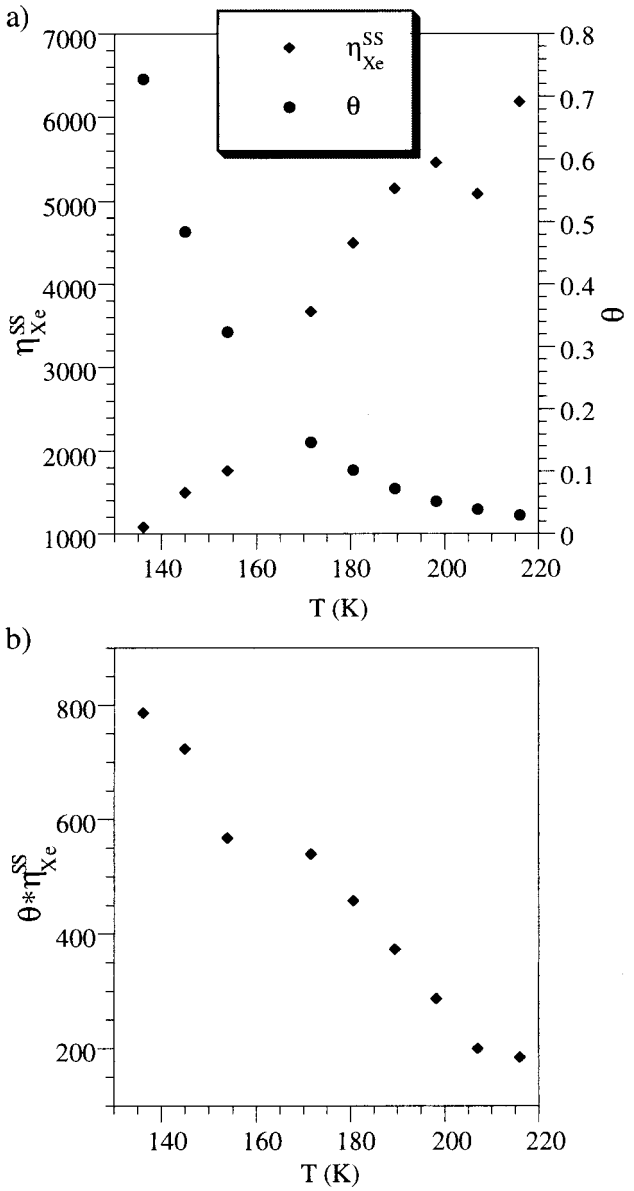

Figure 5. Variation with temperature in (a) xenon surface coverage, θ, and steady-state polarization, η^{SS}_{Xe}, (b) the effective steady-state polarization of surface ^{129}Xe nuclei.

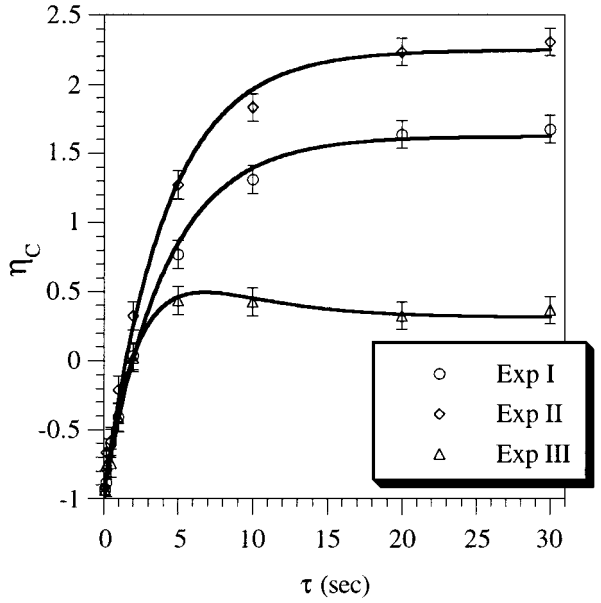

Figure 6. The polarization enhancement data at 136 K for Experiments I (open circle), II (open diamond), and III (open triangle). The fits of the experimental data are shown as solid lines with Experiment I fit to eq 7b, Experiment II fit to eq 10b, and Experiment III fit to eqs 16 and 17.

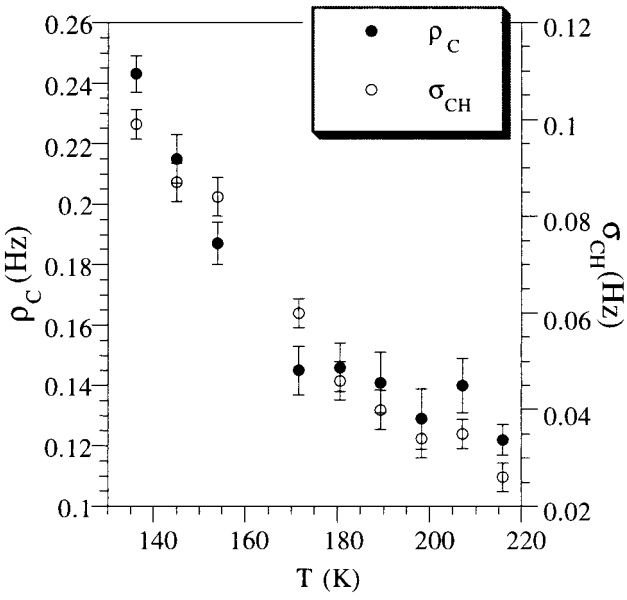

Figure 7. Carbon auto-relaxation (ρ_C) and proton−carbon cross-relaxation (σ_{CH}) rate constants as a function of temperature. Rate constants were derived from least-squares fits of Experiment I data (see text).

decreasing temperature, the adsorbed peak shifted further downfield from the gas-phase peak. Comparison of the integrated intensity of the adsorbed peak with that of a standard thermally polarized sample (natural abundance Xe adsorbed in zeolite Na-Y, the adsorbed peak accounted for 87% of the xenon present at the pressures used in the sealed sample) yielded the surface polarization. Also displayed in Figure 5a are the steady-state surface polarizations as determined for the temperature range of interest. Over the studied temperature range, the surface polarization approaches but never equals the gas-phase polarization[48] of 4.5% ($\eta_{Xe}^{OP} = 10000$ at 55 MHz for ^{129}Xe). The increase in surface polarization occurs with increasing temperature and decreasing coverage. The result of the competition between these two trends is shown in Figure 5b, which displays the temperature dependence of the product of surface coverage and the steady-state polarization. This effective surface xenon magnetization does not change as drastically with temperature as the polarization shown in Figure 5a.

Spin counting experiments were conducted using a known amount of hexamethylbenzene (HMB) as the ^{13}C standard. Comparison of the ^{13}C signal from HMB with the ^{13}C signal of the chemisorbed methanol yielded a surface content of 1.5×10^{19} molecules. The grade M-5 Cab-O-Sil was determined to have a surface area of 175 m^2/g based on nitrogen BET. For 25 mg of silica, the total surface area is 4.4 m^2, which yields 2×10^{19} hydroxyl groups, based on a hydroxyl coverage of 4.6 groups per nm^2.[51] This hydroxyl coverage was also confirmed through spin counting experiments. The coverage by the methoxy groups was determined to be 75%.

From the time-dependent signal intensity of the three experiments discussed above, auto-relaxation (ρ_C, ρ_H) and cross-relaxation parameters (σ_{CH}, σ_{CXe}, σ_{HXe}) were determined via least-squares fitting methods. An example of the quality of the fits obtained for the data collected at 136 K is shown in Figure 6. The carbon auto-relaxation rate constants and unscaled proton−carbon cross-relaxation rate constants determined from Experiment I and fit using eq 7b are plotted versus temperature in Figure 7. Both the carbon auto-relaxation and proton−carbon cross-relaxation rate constants appear to decrease approximately linearly with increasing temperature. Xenon−carbon cross relaxation rate constants, σ_{CXe}, were determined from the fit of Experiment II data to eq 10b and are plotted versus temperature in Figure 8a along with the xenon−proton cross-relaxation rate constants, σ_{HXe}, determined in the fit of Experiment III data to eqs 16 and 17. The cross-relaxation rate constants demonstrate a seemingly exponential increase with decreasing temperature. Since the xenon coverage varies with temperature, the number of carbon and proton nuclei involved in cross relaxation will vary as well. To account for these differences, the xenon−carbon and xenon−proton cross relaxation rates were scaled by the coverage; the resulting values are shown in Figure 8b. The rate constants, σ_{CXe} and σ_{HXe}, when scaled for xenon surface coverage, show temperature dependencies typical for cross-relaxation. The values traverse a maximum as the temperature, or more directly the xenon surface correlation time, changes. All the rate constants along with errors for the values, quoted with 95% confidence limits, are tabulated in Supplementary Information along with the proton auto-relaxation rate constants determined through saturation recovery experiments.

From the solutions to the differential equations describing the three experiments, the maximum steady-state intensity for each case can be calculated. These calculated maximum steady-state enhancements are plotted as a function of temperature in Figure 9. The enhancement for Experiment II traverses a maximum at 172 K. This effect is less pronounced for the other two experiments, between 135 and 216 K, the enhancements do not vary by more than a factor of 2. The enhancements all decrease to low values at the higher temperatures.

Discussion

From eqs 11 and 19 that describe the polarization enhancements for the two SPINOE experiments, it is apparent that three factors—polarization, auto-relaxation, and cross-relaxation—combine to give the observed signal gains. Modification of these factors is necessary for any improvement to the SPINOE enhancement. While surface xenon polarization influences the magnitude of the SPINOE enhancement, surface polarization depends on surface coverage. The magnitude and sign of the

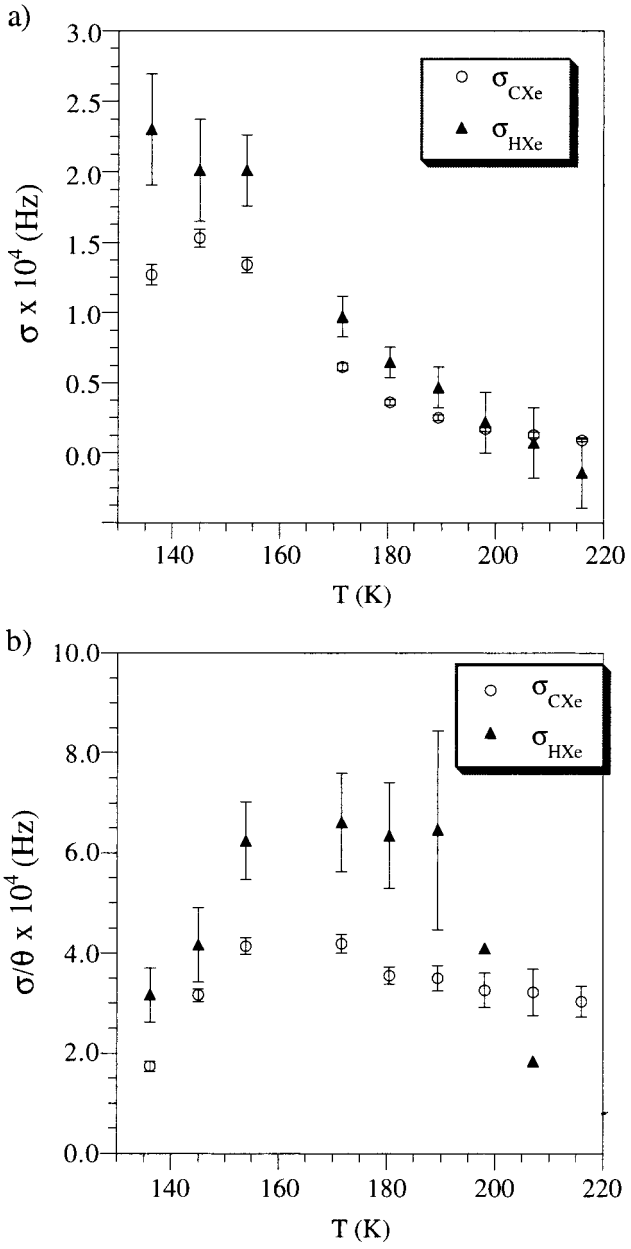

Figure 8. Variation with temperature of (a) xenon−proton and xenon−carbon cross-relaxation rate constants, (b) the coverage scaled xenon−proton and xenon−carbon cross-relaxation rate constants. Rate constants were derived from least-squares fits of Experiment II and III data (see text). Error bars for two high-temperature rate constants were removed for clarity.

cross-relaxation processes depend on the correlation time of the xenon interaction with the surface nuclei. Surface diffusion defines this correlation time and thus affects the SPINOE enhancements. The temperature dependence of the xenon surface dynamics and cross-relaxation dynamics also plays an important role. And finally, independent of the surface, auto-relaxation rates of the carbon nuclei can be altered to affect the enhancement. Improvements in the SPINOE that may be possible from the modification of these factors are discussed below.

Xenon Coverage. One interesting result of this study is that the observed ^{13}C maximum enhancement of 3.4 occurs at 172 K, and not at the lowest temperature in the study where xenon coverage is the highest. While the xenon surface polarization and coverage control the number of carbon atoms enhanced, the temperature of the maximum in xenon−carbon cross-relaxation rate constants governs the temperature of the observed

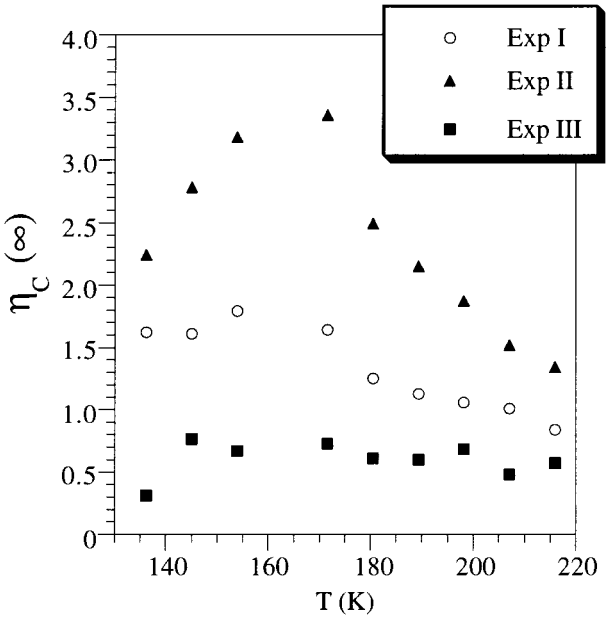

Figure 9. Calculated steady-state enhancements, $\eta_C(\infty)$, of the ^{13}C signal of the methyl group carbon at various temperatures for Experiments I, II, and III.

maximum in the SPINOE enhancements. From Figure 5b, it is clear that the effective surface polarization changes only by approximately 25% over the same temperature range that the cross-relaxation rate constants double in magnitude, as seen in Figure 8b. Thus, the rate of change in the cross-relaxation rate constants controls the rate of change in the low-temperature SPINOE enhancements. Nevertheless, xenon coverage and polarization do affect the size of the observed SPINOE. Surface polarization and coverage show opposite dependencies on temperature. Higher coverage reduces the rate at which surface xenon is replenished relative to its effective relaxation time, resulting in a lower steady-state surface polarization. Due to the limited laser power used in these experiments, it is not possible to increase the xenon gas flow rate because that would lower the polarization of the xenon delivered to the rotor. As the time required for replacement of the xenon increases, the increased surface interaction leads to more relaxation. The loss in polarization at lower temperatures is not as great as the loss in coverage at higher temperatures such that the effective polarization of the xenon, as measured by the number of carbon atoms it interacts with, varies inversely with temperature.

Cross-Relaxation. A comparison of the steady-state polarization enhancements from the three experiments, displayed in Figure 9, clearly shows that Experiment II delivers the largest enhancement at all the temperatures studied. Superior enhancements via this method have been observed previously at low temperatures when the hydrogen nuclei are saturated.[40,41] The large enhancement is the result of the sum of the two NOE effects. Separately, the xenon−carbon SPINOE and proton−carbon NOE enhancements are similar in magnitude at all temperatures. Both enhancements exceed the steady-state values for the full SPINOE (Experiment III) at all the temperatures studied.

The full SPINOE steady-state enhancements are limited by negative polarization enhancement from the protons. The "leakage" term in the steady-state enhancement (eq 19), $\gamma_{Xe}/\gamma_C \cdot \sigma_{CH} \cdot \sigma_{HXe} \cdot \eta_{Xe}^{SS}/\rho_C \cdot \rho_H$, is dependent on both proton−carbon and xenon−proton cross-relaxation and it has a sign opposite to the xenon−carbon SPINOE. The result is a broad maximum

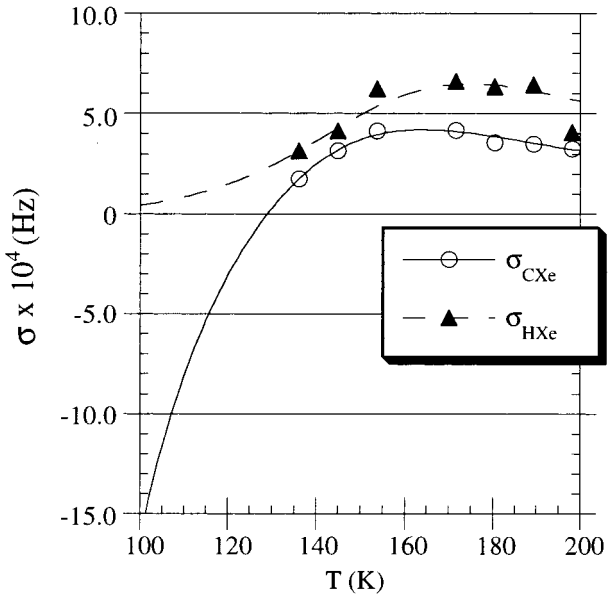

Figure 10. Extrapolated xenon−proton and xenon−carbon cross-relaxation rate constants predicted from fits of the displayed higher temperature rate constant data.

over which the enhancement changes little, varying only between 0.6 and 0.8.

Both Experiment II and III consist of a xenon−carbon SPINOE that is enhanced by the addition of polarization from the proton−carbon NOE. The difference lies in the enhancement of the proton−carbon NOE. A decrease of η_C would not occur if the resulting sign of the xenon−proton SPINOE enhancement were positive. This would require the sign of σ_{HXe} to be negative. An alternative option would be to have a negative NOE, resulting from $\sigma_{CH} < 0$; the leakage term would then yield a positive value in eq 19. However, both conditions are not possible. Cross-relaxation between protons and nuclei with smaller gyromagnetic ratios always results in rates that never change sign regardless of the correlation time.[52] Only σ_{CXe} may experience a change in sign at longer correlation times. Changing the sign of the carbon−xenon interaction would then allow for the polarization from the protons to add constructively, yielding a larger SPINOE. Ironically, the change in sign would then result in smaller SPINOE enhancements for Experiment II (eq 10) as the xenon−carbon SPINOE and proton−carbon NOE would now have opposite signs (since $\gamma_{Xe} < 0$).

Hopping Model. The motion of the adsorbed xenon across the silica surface can be thought of as a series of hops from one methoxy group to another. This motion makes the dipolar coupling between the ^{129}Xe nuclei and the ^{13}C and ^{1}H nuclei time-dependent, allowing for cross-relaxation to occur. The scaled cross-relaxation rate constants can be fit to extract the dipolar distance between the xenon and carbon atoms, the activation energy for xenon motion across the surface, and the time constant for xenon motion. The equation describing cross-relaxation[53] is

$$\sigma_{IS} = \left(\frac{\mu_0}{4\pi}\right)^2 \cdot \frac{\hbar^2 \cdot \gamma_I^2 \cdot \gamma_S^2}{10 \cdot r_{IS}^6} \cdot \left(\frac{6 \cdot \tau_c}{1 + (\omega_I + \omega_S)^2 \cdot \tau_c^2} - \frac{\tau_c}{1 + (\omega_I - \omega_S)^2 \cdot \tau_c^2}\right) \quad (20)$$

The correlation time can be assumed to have an Arrhenius temperature dependence. The nonlinear least-squares fit, shown in Figure 10, yields an internuclear distance of 3.6 ± 0.02 Å, activation energy of 5.4 ± 0.2 kJ/mol, and a τ_0 of 2.1 ± 0.4 × 10^{-11} s. Given that the radii of a carbon atom and a xenon atom are approximately 0.77 and 2.2 Å, respectively, a dipolar distance of 3.6 Å is reasonable. Since the approach of the xenon atom is blocked by the hydrogen atoms of the methyl group, the distance between the xenon and carbon atoms would be expected to be greater than the sum of the radii. Activation energies of similar value (5.1 ± 0.9 kJ/mol) have been observed for surface diffusion in Vycor glass.[54] With a methoxy coverage of 75%, the average distance between methoxy species on the surface is approximately 6 Å. At 150 K the correlation time for a xenon atom is 1.6 ± 0.4 × 10^{-9} s, which results in a surface diffusion rate on the order of 10^{-10} m^2/s. Diffusion rates for xenon in Vycor glass, extrapolated to 150 K using the parameters measured by Moudrakovski and co-workers,[54] are 5 × 10^{-9} m^2/s. The similarity in the magnitude of the diffusion coefficients further supports the model of xenon hopping across the surface.

The coverage scaled cross-relaxation rate constants for the proton−xenon interaction can also be fit using an Arrhenius model for the temperature dependence. Assuming that a xenon atom interacts with the three protons of the methyl group, the fit, shown in Figure 10, yielded a distance of 4.60 ± 0.01 Å, activation energy of 5.7 ± 0.5 kJ/mol, and a τ_0 of 1.2 ± 0.5 × 10^{-11} s. The dipolar distance of the xenon−proton interaction is longer than what is expected based on the results for the xenon−carbon cross-relaxation and based on the model of xenon atoms colliding with the methyl group. One possible explanation for this observation is the fact that rotation of the methyl group is fast, which reduces the effective dipolar coupling and results in a longer calculated dipolar distance. The decrease in proton−carbon cross-relaxation rate with increasing temperature would seem to indicate that the methyl group rotation is in the fast motion limit. σ_{HXe} values of this reduced magnitude, as compared to values expected for short xenon−hydrogen distances, have been observed previously.[33,35] Another possibility is that the xenon atom may prefer to reside on the silica surface between hops and not on the methyl group itself; a situation depicted in Figure 1. In this arrangement, the xenon atom would be closer to the carbon atom than the three hydrogen atoms. The farthest hydrogen atom opposite the xenon would be approximately 1 Å more distant than the carbon atom. The fast rotation of the methyl group would average the xenon−proton distance yet the dipolar distance would be longer than if the xenon atom had collided directly with the methyl group. Nevertheless, the results of the fits do model the low-temperature data well and should be able to predict the cross-relaxation rate constants at even lower temperatures. At higher temperatures, large errors exist for σ_{HXe} since the increased percent errors of the other data parameters (σ_{CXe} and ρ_C) and the smaller SPINOE enhancement for Experiment III make determination of the small xenon−proton interaction difficult.

Possible Improvements. With the two cross-relaxation rate constants modeled as a function of temperature, the temperatures at which significant SPINOE magnitudes exist can be determined. The challenge is to find a temperature for which the sign of σ_{CXe} will be negative and the magnitudes of both σ_{CXe} and σ_{HXe} will be significant. From Figure 10, the appropriate temperature would appear to be between 120 and 128 K. This temperature range is unfortunately unrealistic for our current experimental setup. At temperatures below 132 K, solid xenon formation on the silica surface is observed under continuous flow conditions. The rate of surface replenishment of the hyperpolarized xenon decreases due to the restricted diffusion

of the solid and would limit the effectiveness of the continuous flow system to maintain a large steady-state surface xenon polarization. As well, the mobile adsorbed xenon reaches a surface coverage at these temperatures that exceeds one monolayer, according to BET theory, unless the xenon partial pressure is very low. Multiple monolayers would also decrease the xenon replenishment rate due to restricted diffusion between the layers resulting in a severe decrease in the xenon steady-state surface polarization. Nevertheless, assuming a steady-state surface xenon polarization could be maintained at these low temperatures, a prediction of the SPINOE enhancement is possible. Using the auto-relaxation rates for the lowest temperatures (which probably only introduce about 10% error) and the predicted cross-relaxation rates for those temperatures, the maximum SPINOE enhancement is about −1.4. The negative enhancement (since $\gamma_{Xe} < 0$) is almost double the maximum positive value observed.

While the lower temperature SPINOE is not possible for this sample, other materials with higher heats of adsorption may make SPINOE enhancements of this magnitude feasible. The activation energy for surface diffusion is expected generally to be 10%−20% of the adsorption energy.[55] With a larger heat of adsorption, longer correlation times should occur at temperatures above that necessary for the formation of solid xenon. These longer correlation times for xenon hopping would give the necessary sign and magnitude for σ_{CXe} and σ_{HXe} to yield larger SPINOE enhancements. Under the same conditions used in the above calculation, an increase in the activation energy of xenon hopping by 400 J/mol would result in a shift of the cross-relaxation rates such that an enhancement of −1.4 would now be observed at 129 K. Increasing the activation energy by 1 kJ/mol causes the SPINOE enhancement of −1.4 to occur at 143 K with the enhancement increasing as the temperature decreases: −2.4 at 136 K and −5.8 at 120 K. At the lower temperatures, the contribution from the protons becomes reduced such that the enhancements are primarily due to the xenon−carbon SPINOE. Various surfaces exist which have the necessary larger heat of adsorption. Some of these materials are NaCl (19.2 kJ/mol),[56] silica-supported TiO_2 monolayers (∼30 kJ/mol),[57] Pt (23.8 kJ/mol),[58] and Al (18.3 kJ/mol),[59] which could serve as potential substrates for significant SPINOE-induced enhancements of adsorbed molecules.

Ultimately, the most certain way of eliminating the polarization "leakage" is to eliminate the protons entirely by isotopic substitution with deuterium. Clearly the loss of the protons will remove the proton−carbon NOE which serves as the mechanism to reduce polarization enhancement. The isotopic substitution will also affect the carbon auto-relaxation since the carbon−proton dipolar coupling is a major relaxation pathway. Thus the exchange would decrease the relaxation rate of carbon, further increasing the enhancement from the xenon−carbon SPINOE. Saturation of the protons will also eliminate the leakage as demonstrated by Experiment II and allows for the NOE to add to the enhancement. However, the proton saturation will not affect the carbon auto-relaxation rate since the dipolar coupling is still present. Typically, the loss of dipolar coupling to protons results in a rate change of an order of magnitude increasing the SPINOE enhancement by a similar amount.[41] In addition, the use of alternative substrates to increase the magnitude of the xenon−carbon cross-relaxation rates at low temperatures would further increase the SPINOE enhancement by a factor of 2 or 3. Finally, any increase in the surface xenon polarization will result in a larger enhancement for all versions of the SPINOE experiment. Most recently, we have been able to increase our gas-phase polarization[48] to 16% ($\eta_{Xe}^{OP} = 36000$).[60] The greater polarization should be reflected in the surface polarization as well and increase any SPINOE enhancement.

Conclusions

The temperature dependence of the xenon−carbon SPINOE and the full SPINOE experiments were observed with lower temperatures yielding the largest enhancements. Due to the loss of polarization from the leakage inherent in the full SPINOE experiment, the enhancements vary little with temperature and never exceed 0.8. Xenon−carbon SPINOE enhancements, in contrast, are larger, reaching a maximum of 3.4, due to the elimination of the proton leakage. The temperature dependence of the enhancements was found to correlate with the temperature dependence of the cross-relaxation rates involving the xenon nuclei. These cross-relaxation rate constants are a function of the xenon hopping correlation time and therefore a function of the xenon surface diffusion. Reduction in the xenon surface diffusion rate would lead to larger negative values for the xenon carbon cross-relaxation rate constant, σ_{CXe}, and thus larger negative enhancements. Reversal of the sign of the xenon−carbon SPINOE enhancements would also allow for the constructive addition of polarization from the methyl group protons, also enhanced by the polarized xenon, in the full SPINOE experiment. The use, as substrates, of surfaces with heats of adsorption higher than those for silica should result in higher activation energies for diffusion and thus reduced xenon mobility. While mobility is key to the success of SPINOE due to the need of a fluctuating dipole for relaxation to occur, the rate of diffusion on the silica surface is still too high to achieve large SPINOE enhancements. Alternate substrates with higher diffusion activation energies should yield large negative SPINOE gains, with predicted gains up to −5.8. Reduction in xenon mobility combined with increased xenon polarization (16% or higher with more powerful lasers) and with reduced proton dipolar coupling (decreasing ^{13}C relaxation by a factor of 10) should allow increases over the current SPINOE enhancements by almost 2 orders of magnitude**,** vastly improving the signal gain possibilities of this method.

Acknowledgment. J.S. thanks Purdue Research Foundation for financial support. Support for this research from the National Science Foundation (CHE95-31693), the A. P. Sloan Foundation, and the Research Corporation is gratefully acknowledged.

Supporting Information Available: Supporting Information: The rate constants along with errors for the values, quoted with 95% confidence limits, are tabulated along with the proton auto-relaxation rate constants determined through saturation recovery experiments.. This material is available free of charge via the Internet at http://pubs.acs.org.

References and Notes

(1) Ansermet, J.-Ph.; Slichter, C. P.; Sinfelt, J. H. *Prog. NMR Spec.* **1990**, *22*, 401.

(2) Zilm, K. W.; Bonneviot, L.; Haller, G. L.; Han, O. H.; Kermarec, M. *J. Phys. Chem.* **1990**, *94*, 8495.

(3) Klinowski, J. *Chem. Rev.* **1991**, *91*, 1459.

(4) Fyfe, C. A.; Feng, Y.; Grondey, H.; Kokotailo, G. T.; Gies, H. *Chem. Rev.* **1991**, *15*, 1525.

(5) *NMR Techniques in Catalysis*; Bell, A. T., Pines, A., Eds.; Marcel Dekker Inc: New York, 1994.

(6) Pfeifer, H. *NMR—Basic Principles and Progress* **1994**, *31*, 31.

(7) Eckert, H. *Curr. Opin. Solid State Mater. Sci.* **1996**, *1*, 465, and references within.

(8) Haw, J. F.; Nicholas, J. B.; Xu, T.; Beck, L. W.; Ferguson, D. B. *Acc. Chem. Res.* **1996**, *29*, 259.

(9) Wu, J. J.; Day, J. B.; Franaszczuk, K.; Montez, B.; Oldfield, E.; Wieckowski, A.; Vuissoz, P. A.; Ansermet, J. P. *J. Chem. Soc., Faraday Trans.* **1997**, *93*, 1017.
(10) Haw, J. F.; Xu, T. *Adv. Catal.* **1998**, *42*, 115.
(11) Hwang, S. J.; Petucci, C.; Raftery, D. *J. Am. Chem. Soc.* **1998**, *120*, 4388.
(12) Pilkenton, S.; Hwang, S. J.; Raftery, D. *J. Phys. Chem. B* **1999**, *103*, 11152.
(13) Walker, T. G.; Happer, W. *Rev. Mod. Phys*. **1997**, *69*, 629, and references therein.
(14) Raftery, D.; Chmelka, B. F. *NMR—Basic Principles and Progress* **1994**, *30*, 111.
(15) Pietrass, T. *Colloid Surface A* **1999**, *158*, 51.
(16) Brunner, E. *Magn. Reson. Chem.* **1999,** *37*, S14.
(17) Raftery, D.; Long, H.; Meersmann, T.; Grandinetti, P. J.; Reven, L.; Pines, A. *Phys. Rev. Lett.* **1991**, *66*, 584.
(18) Albert, M. S.; Cates, G. D.; Driehuys, B.; Happer, W.; Saam, B.; Springer, C. S., Jr.; Wishnia, A. *Nature* **1994**, *370*, 199.
(19) Middleton, H.; Black, R. D.; Saam, B.; Cates, G. D.; Cofer, G. P.; Guenther, R.; Happer, W.; Hedlund, L. W.; Johnson, G. A.; Juvan, K.; Swartz, J. *Magn. Reson. Med.* **1995**, *33*, 271.
(20) Bowers, C. R.,; Pietrass, T.; Barash, E.; Pines, A.; Grubbs, R. K.; Alivisatos, A. P. *J. Phys. Chem.* **1994**, *98*, 9400.
(21) Song, Y.-Q.; Gaede, H. C.; Pietrass, T.; Barrall, G. A.; Chingas, G. C.; Ayers, A.; Pines, A. *J. Magn. Reson. A* **1995**, *115*, 127.
(22) Pietrass, T.; Gaede, H. C.; Bifone, A.; Pines, A.; Ripmeester, J. A. *J. Am. Chem. Soc.* **1995**, *117*, 7520.
(23) Goodson, B. M.; Song, Y.-Q.; Taylor, R. E.; Schepkin, V. D.; Brennan, K. M.; Chingas, G. C.; Budinger, T. F.; Navon, G.; Pines, A. *Proc. Natl. Acad. Sci. U.S.A.* **1997**, *94*, 14725.
(24) Tseng, C. H.; Wong, G. P.; Pomeroy, V. R.; Mair, R. W.; Hinton, D. P.; Hoffmann, D.; Stoner, R. E.; Hersman, F. W.; Cory, D. G.; Walsworth, R. L. *Phys. Rev. Lett.* **1998**, *81*, 3785.
(25) Luhmer, M.; Goodson, B. M.; Song, Y.-Q.; Laws, D. D.; Kaiser, L.; Cyrier, M. C.; Pines, A. *J. Am. Chem. Soc.* **1999**, *121*, 3502.
(26) Jänsch, H. J.; Hof, T.; Ruth, U.; Schmidt, J.; Stahl, D.; Fick, D. *Chem. Phys. Lett.* **1998**, *296*, 146.
(27) Moudrakovski, I. L.; Lang, S.; Ratcliffe, C. I.; Simard, B.; Santyr, G.; Ripmeester, J. A. *J. Magn. Reson.* **2000**, *144*, 372.
(28) Long, H. W.; Gaede, H. C.; Shore, J.; Reven, L.; Bowers, C. R.; Kritzenberger, J.; Pietrass, T.; Pines, A. *J. Am. Chem. Soc.* **1993**, *115*, 8491.
(29) Gaede, H. C.; Song, Y.-Q.; Taylor, R. E.; Munson, E. J.; Reimer, J. A.; Pines, A. *Appl. Magn. Reson.* **1995**, *8*, 373.
(30) Driehuys, B.; Cates, G. D.; Happer, W.; Mabuchi, H.; Saam, B.; Albert, M. S.; Wishnia, A. *Phys. Lett. A* **1993**, *184*, 88.
(31) Bowers, C. R.; Long, H. W.; Pietrass, T.; Gaede, H. C.; Pines, A. *Chem. Phys. Lett.* **1993**, *205*, 168.
(32) Navon, G.; Song, Y.-Q.; Rõõm, T.; Appelt, S.; Taylor, R. E.; Pines, A. *Science* **1996**, *271*, 1848.
(33) Rõõm, T.; Appelt, S.; Seydoux, R.; Hahn, E. L.; Pines, A. *Phys. Rev. B* **1997**, *55*, 11604.
(34) Raftery, D.; MacNamara, E.; Fisher, G.; Rice, C. V.; Smith, J. *J. Am. Chem. Soc.* **1997**, *119*, 8746.
(35) Song, Y.-Q.; Goodson, B. M.; Taylor, R. E.; Laws, D. D.; Navon, G.; Pines, A. *Angew. Chem., Int. Ed. Engl.* **1997**, *36*, 2368.
(36) Brunner, E.; Seydoux, R.; Haake, M.; Pines, A.; Reimer, J. A. *J. Magn. Reson.* **1998**, *130*, 145.
(37) Brunner, E.; Haake, M.; Pines, A.; Reimer, J. A.; Seydoux, R. *Chem. Phys. Lett.* **1998**, *290*, 112.
(38) Pietrass, T.; Seydoux, R.; Pines, A. *J. Magn. Reson.* **1998**, *133*, 299.
(39) MacNamara, E.; Fisher, G.; Smith, J.; Rice, C. V.; Hwang, S.-J.; Raftery, D. *J. Phys. Chem. B* **1999**, *103*, 1158.
(40) Seydoux, R.; Pines, A.; Haake, M.; Reimer, J. A. *J. Phys. Chem. B* **1999**, *103*, 4629.
(41) MacNamara, E.; Rice, C. V.; Smith, J.; Smith, L. J.; Raftery, D. *Chem. Phys. Lett.* **2000**, *317*, 165.
(42) Song, Y.-Q. *Concepts Magn. Reson.* **2000**, *12*, 6.
(43) The forward and reverse rate constants involved in the polarization transfer are related by $\sigma_{IS} = N_S/N_I \cdot S \cdot (S + 1)/I \cdot (I + 1) \cdot \sigma_{SI}$, where I and S refer to the spin of the nucleus, and N_S and N_I refer to the relative number of nuclei involved in the cross-relaxation.
(44) Noggle, J. H.; Schirmer, R. E. *The Nuclear Overhauser Effect*: Academic Press: New York, 1971.
(45) Dettman, J. W. *Introduction to Linear Algebra and Differential Equations*; McGraw-Hill: New York, 1974.
(46) Driehuys, B.; Cates, G. D.; Miron, E.; Sauer, K.; Waler, D. K.; Happer, W. *Appl. Phys. Lett.* **1996**, *69*, 1668.
(47) Hunger, M.; Horvath, T. *J. Chem. Soc. Chem. Commun.* **1995**, 1423.
(48) Nuclear spin polarization for a spin-1/2nucleus is defined as $|N_\alpha - N_\beta/N_\alpha + N_\beta| \cdot 100\%$ and is an absolute value unlike η which is defined with respect to the thermal Boltzmann polarization. N_α and N_β represent the populations of the +1/2and -1/2energy levels, respectively.
(49) Bielecki, A.; Burum, D. P. *J. Magn. Reson. Ser. A* **1995**, *116*, 215.
(50) Brunauer, S.; Emmett, P. H.; Teller, E. *J. Am. Chem. Soc.* **1938**, *60*, 309.
(51) Sneh, O.; George, S. M. *J. Phys. Chem.* **1995**, *99*, 4639.
(52) Neuhaus, D.; Williamson, M. P. *The Nuclear Overhauser Effect in Structural and Conformational Analysis*; VCH: New York, 1989.
(53) Slichter, C. P. *Principles of Magnetic Resonance*; Springer-Verlag: Berlin, 1990.
(54) Moudrakovski, I. L.; Sanchez, A.; Ratcliffe, C. I.; Ripmeester, J. A. *J. Phys. Chem. B* **2000**, *104*, 7306.
(55) Somorjai, G. A. *Chemistry in Two Dimensions: Surfaces*; Cornell University Press: Ithaca, NY, 1981.
(56) Gerlach, R.; Graham, A. P.; Toennies, J. P.; Weiss, H. *J. Chem. Phys.* **1998**, *109*, 5319.
(57) Terskikh, V. V.; Seidl, M.; Knozinger, H. *Colloid Surf. A* **1999**, *158*, 249.
(58) Sneh, O.; Geroge, S. M. *J. Chem. Phys.* **1994**, *101*, 3287.
(59) Schneider, U.; Castro, G. R.; Isern, H.; Janssens, T.; Wandelt, K. *Surf. Sci.* **1991**, *251*, 551.
(60) Smith, J.; Smith, L. J.; Knagge, K.; MacNamara, E.; Raftery, D. Submitted.